Interaction between Energy Leakage, Photovoltaic Replenishment, and Workload in a Green IoT Device

Preprint · February 2025

DOI: 10.13140/RG.2.2.30038.15682

6 authors, including:

Godlove Suila Kuaban
Polish Academy of Sciences
45 PUBLICATIONS **234** CITATIONS
SEE PROFILE

Erol Gelenbe
Polish Academy of Sciences
892 PUBLICATIONS **25,237** CITATIONS
SEE PROFILE

Piotr Pecka
Polish Academy of Sciences
17 PUBLICATIONS **41** CITATIONS
SEE PROFILE

Valery Nkemeni
University of Buea
18 PUBLICATIONS **48** CITATIONS
SEE PROFILE

Interaction between Energy Leakage, Photovoltaic Replenishment, and Workload in a Green IoT Device

Godlove Suila Kuaban[a,*], Tadeusz Czachórski[a], Erol Gelenbe[a], Piotr Pecka[a], Valery Nkemeni[b], Piotr Czekalski[c]

[a] *Institute of Theoretical and Applied Informatics, Polish Academy of Sciences, Baltycka 5, Gliwice, 44–100, Poland*
[b] *Department of Computer Engineering, Faculty of Engineering and Technology, University of Buea, Molyko, Buea, P.O. Box 63, Cameroon*
[c] *Faculty of Automatic Control, Electronics and Computer Science, Silesian University of Technology, Akademicka 16, Gliwice, 44–100, Poland*

Abstract

Despite significant advancements in green IoT design frameworks aimed at minimizing energy consumption, extending node lifetimes, reducing carbon footprints, and enhancing sustainability, energy losses due to imperfections in energy storage systems (ESS)—such as batteries, capacitors, and supercapacitors—remain a critical challenge. These inefficiencies degrade the overall energy performance of IoT nodes and must be carefully accounted for in energy-efficient system design. This paper analyzes the impact of ESS non-idealities on green IoT nodes, focusing on energy leakage and its effects on key performance metrics, including service outage probability, node lifetime distribution, and the time-dependent mean number of energy packets (EPs) in the ESS. To mitigate energy losses from leakage, we explore two key strategies: (i) Enhancing energy generation by increasing energy harvester capacity (e.g., deploying additional solar panels or higher-efficiency alternatives). (ii) Reducing energy consumption by implementing ESS energy thresholds that transition nodes into low-power states when energy levels drop below predefined limits. By addressing ESS imperfections and optimizing energy management strategies, this work aims to enhance the sustainability, reliability, and efficiency of green IoT nodes by analyzing the interplay between energy leakage, workload-driven energy demand, and photovoltaic energy harvesting.

Keywords: Green IoT; energy storage systems; energy harvesting; energy leakage; energy-saving strategies; time-dependent analysis.

*Corresponding author.
Email address: gskuaban@iitis.pl (Godlove Suila Kuaban)

1. Introduction

The energy performance of practical energy storage systems (ESS) for the Internet of Things (IoT) and embedded systems is often influenced by various imperfections or non-idealities. These include issues such as capacity degradation over time (due to increased charge-discharge cycles), energy leakage, charge recovery effects, and battery degradation. These practical imperfections, combined with fluctuations in the energy demand of IoT nodes, can lead to increased energy consumption, a higher carbon footprint, and reduced reliability. Specifically, they increase the likelihood of energy-related service outages and shorten the node's lifespan. To mitigate these impacts, it is essential to incorporate phenomena that cause these non-idealities, such as capacity drop, energy leakage, and charge recovery, into the energy storage system models [1]. However, incorporating such processes into the models also increases their complexity. This paper focuses on evaluating the impact of energy leakage on the energy performance of green IoT nodes.

In ideal conditions, the potential of a battery remains constant. However, in reality, its potential decreases over time, even when it is not under load (as in the case of IoT nodes), resulting in self-discharge. The current associated with this self-discharge is called leakage current. The rate of leakage (or self-discharge) may be influenced by factors such as chemical reactions, thermal or kinetic energy loss [2], manufacturing defects, impurities, and ageing (which can degrade internal materials and increase leakage current). This means that energy continues to leak from the battery even when the device is in deep sleep mode, despite efforts to minimise energy depletion.

Although capacitors and supercapacitors are often recommended as alternatives due to their high power densities and long cycle lives [1], they also experience energy leakage due to significant self-discharge. As we explore the impact of energy-saving strategies and energy harvesting on achieving the green IoT vision, it is crucial to account for imperfections such as energy leakage in the energy storage system models.

The growing interest in green IoT design stems from the increasing demand for sustainability in the rapidly expanding IoT industry [3]. Green IoT [4, 5, 6] refers to the design and implementation of IoT systems that promote environmental sustainability by minimising energy consumption and reducing pollutants (such as CO2, electronic waste, and other toxic substances) produced during the manufacturing, deployment, and operation of IoT systems and related infrastructures (e.g., edge computing, core networks, cloud computing). Key aspects of green IoT include using energy-efficient devices, reducing carbon footprints, utilising renewable energy sources, and optimising resource usage to minimise environmental degradation.

Green IoT is an evolving field, and numerous techniques are being explored to reduce energy consumption and pollution in IoT systems. Many of these techniques focus on reducing energy consumption in computing and communication nodes, particularly those powered by off-grid energy sources (e.g., energy storage systems like batteries, capacitors, or supercapacitors) and fossil-fuel-based

energy. Reducing energy consumption and relying on renewable energy sources can also reduce operational costs, improving the financial sustainability of IoT infrastructures, especially as energy costs rise. Energy-efficient strategies for green IoT include duty cycling, reducing packet sizes, optimising transceivers, energy-aware routing, adaptive sensing, reducing protocol overhead, voltage and frequency control [7, 8], energy-efficient hardware and software design [9, 8], and the integration of renewable energy into IoT systems.

In most green IoT systems, ESS (e.g., batteries, capacitors, or supercapacitors) store excess energy harvested from renewable energy sources to power IoT nodes when those sources are unavailable. Given the intermittent nature of renewable energy sources, energy storage is indispensable. The energy consumption of IoT nodes can be stochastic, as their energy demand fluctuates over time [10]. Therefore, designing green IoT systems requires optimising the energy demand of nodes, energy production from harvesting systems, and energy capacity from storage systems to enhance the energy performance (efficiency, availability, and sustainability) of IoT nodes.

The design goal is to size the energy harvesting system to meet the node's energy demand during favourable environmental conditions while ensuring sufficient energy storage to avoid energy outages or maximise node lifetime (the time from deployment until the battery is empty and the energy source can no longer meet the node's demands). Over-provisioning energy harvesting and storage may increase costs and affect other design aspects, such as size, weight, mobility, and sustainability. However, under-provisioning may increase the probability of service outages and shorten the node's lifetime [2]. Therefore, realistic models are needed to dimension and evaluate the energy performance of energy production, storage, and consumption systems for green IoT nodes.

When designing green IoT nodes, it is essential to account for energy leakage by properly sizing the energy harvesting and storage systems to compensate for lost energy. This mitigates the impact of leakage on service outage probability and node lifetime. While several studies on energy performance modelling for IoT nodes [11, 12, 3, 13, 14, 15, 16, 17, 18, 19] have overlooked the effects of energy leakage in energy storage systems (ESSs), others have explicitly modeled its impact in wireless communication nodes [2, 20, 1, 21, 22, 23].

A widely used approach for evaluating energy performance in IoT nodes-without focusing on the technical intricacies of energy harvesters, nodes, and storage systems — is to discretize energy into energy packets. The energy packet framework, introduced in [24, 25], leverages queueing theory to model the charging and discharging processes in energy storage systems. Further details on this concept are available in [11, 12, 3].

In this framework, energy harvested and delivered to the battery is treated as energy packet arrivals, while energy consumption is modeled as energy packet servicing. Unlike conventional queueing systems—where the service rate must exceed the arrival rate to prevent overflow—an energy storage system (ESS) must maintain an energy arrival rate exceeding the consumption rate to prevent service outages when the ESS is depleted [2].

Another approach models changes in the energy content of the energy storage

system (ESS) as a continuous stochastic process, such as fluid flow [13, 14, 15] or diffusion processes [17, 18, 19]. A key challenge in incorporating imperfections like energy leakage is that it introduces an additional deterministic or stochastic process that operates alongside conventional arrival and service processes. Moreover, since leakage depends on the current energy level of the ESS, it is not an independent process but is inherently coupled with energy delivery and consumption.

1.1. The main contributions of the paper

Some studies (e.g., [23, 26, 27, 28, 29, 2]) have modelled energy leakage using discrete energy models, treating leakage as energy packets that are lost from the ESS without being used by the IoT node. These models discretise energy into packets and apply queueing theory to analyse the performance of the ESS. However, these studies primarily focused on the interaction between data queues (communication packets) and energy packets rather than investigating the direct impact of energy leakage on energy performance metrics such as service outage probability and node lifetime.

The primary goal of this study is to investigate how non-idealities like energy leakage affect the performance of ESS in green IoT nodes and explore strategies to mitigate energy performance degradation caused by leakage. The main contributions of the paper are as follows:

- We propose an energy packet-based model to evaluate the energy performance of ESS in IoT nodes. We derive analytical solutions for the steady-state distribution of energy packets in the ESS and the probability of service outage. We also perform transient analysis to study the dynamic evolution of ESS energy content over time, providing key performance metrics such as service outage probability, node lifetime, and mean number of energy packets.

- Our study thoroughly examines the impact of energy delivery, consumption, and leakage on ESS performance. We explore different leakage rate models (constant, linear, and exponential) and evaluate their effects on energy performance metrics like service outage probability, node lifetime, and mean number of energy packets. This comprehensive approach provides valuable insights into the impact of energy leakage on the energy performance IoT systems.

- We explore strategies to compensate for the effects of energy leakage on ESS performance, such as increasing the energy production rate. Although ambient energy harvesters produce minimal energy, solar energy harvesters offer scalability and efficiency. We adapt our model to account for energy sources like solar energy, which is available during the day but not at night. Our analytical framework also considers other energy sources like wind and vibration that fluctuate randomly over time. Additionally, we consider energy consumption thresholds that trigger low-power consumption modes in the node to enhance energy efficiency further.

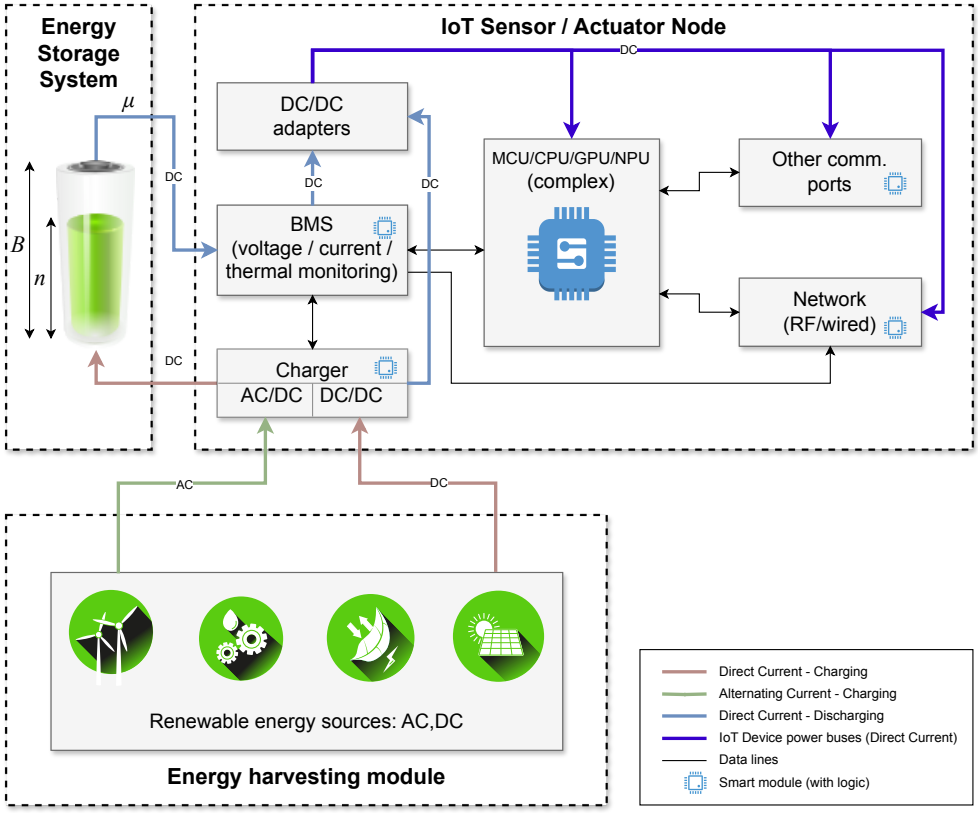

Figure 1: Structure of a self-powered green IoT node

2. The energy model of the self-powered green IoT node

2.1. The energy consumption model of the node

A self-powered green IoT node typically comprises an IoT sensor/actuator, an energy harvesting system, and an energy storage system, as depicted in Fig. 1. The harvested energy, sourced from ambient or external environments, is either directly used to power the IoT device or stored in the energy storage system for later use. When energy harvesting becomes insufficient to meet the node's demands—such as during nighttime in the case of solar energy—the stored energy is utilised to sustain the operation.

Since IoT sensors and actuators perform periodic measurements or control tasks (e.g., meter readings, temperature monitoring) or respond to specific events (e.g., pipeline leak detection, valve control in liquid level monitoring), energy efficiency is crucial. To conserve energy, IoT nodes often switch to low-power sleep modes when not actively operating. The power consumption of a

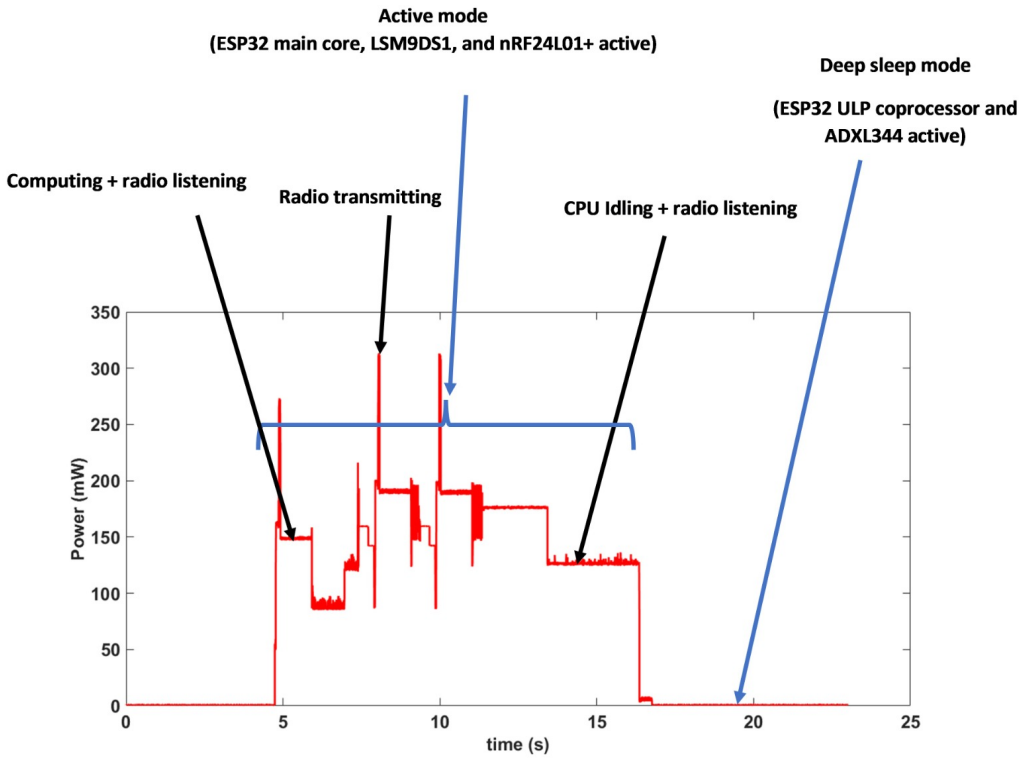

Figure 2: Snapshot of the power profile of an IoT node.

node is given by:

$$P_{\text{node}}(t) = DP_{\text{act}}(t) + (1 - D)P_{\text{sleep}}(t) \tag{1}$$

where

$$D = \frac{t_{\text{act}}}{t_{\text{act}} + t_{\text{sleep}}}$$

t_{act} is the duration in active mode, t_{sleep} is the duration in sleep mode, P_{act} is the power consumption in active mode, and P_{sleep} is the power consumption in sleep mode.Figure 2 presents a snapshot of the power profile of an IoT node, which enters sleep mode whenever it is not engaged in sensing, computing, or communication tasks. The active power consumption is the cumulative sum of power drawn by various modules, including the microcontroller unit, sensor/actuator unit, communication unit, and auxiliary electronic systems such as the power supply.

The power profile highlights the power consumed during active and sleep modes. This profile was obtained from a laboratory testbed comprising two IoT nodes placed 2 meters apart along a 12-meter-long high-pressure plastic

pipe with a 25-mm diameter. To optimise energy consumption, the IoT nodes implement:

- Distributed computing with Kalman filtering, where computing tasks are shared among nodes to reduce individual processing loads.
- Adaptive sensing, which dynamically switches between an energy-efficient but less accurate accelerometer and a high-precision but energy-intensive accelerometer.
- Duty cycling, which forces nodes into sleep mode during idle periods to minimise power consumption.

The mean power consumption over an interval $[0, T]$ is computed as:

$$\mu = \frac{1}{T} \int_0^T P_{\text{node}}(\tau), d\tau. \tag{2}$$

In event-based IoT monitoring systems, nodes remain in sleep mode until triggered by an event. In our scenario, nodes detect leaks and activate high-precision but energy-intensive accelerometer sensors. After capturing vibration data, the nodes perform distributed computing to enhance accuracy, comparing results against predefined leakage thresholds. Here, t_{sleep} follows a stochastic process, as its duration is not deterministic and can be modelled using a probability distribution.

A completely random energy consumption process can be modelled as a Poisson process [30], where energy drawn from the battery follows independent and uniformly distributed patterns. In this case, the energy consumption process is given by:

$$E_{\text{node}} = t_{\text{act}} P_{\text{act}} N_t^{(1/t_i)} \tag{3}$$

where N_t^{μ} represents a standard Poisson process with constant intensity μ. Here, energy is drawn in discrete packets of $t_{\text{act}} P_{\text{act}}$, occurring at intervals that follow an exponential distribution with mean $t_i = t_{\text{act}} + t_{\text{sleep}}$. The mean number of energy packets consumed per time unit over the interval $[0, t_i]$ is:

$$\mu = \frac{t_{\text{act}}}{t_{\text{act}} + t_{\text{sleep}}} \cdot \frac{P_{\text{act}}}{E_p} \tag{4}$$

where E_p denotes the size of an energy packet.

2.2. The energy harvesting model of the node

To enhance reliability, the energy harvesting system may include multiple harvesters, such as photovoltaic and piezoelectric harvesters, which can generate power on the order of a few hundred milliwatts.

Photovoltaic-based energy harvesters capture energy from light sources—either solar or artificial light—and convert it into electrical energy via the photovoltaic effect [31]. The output power of a photovoltaic (PV) array can be derived using

the PV output power model developed by the American National Renewable Energy Laboratory (NREL) [32]. This model has been used in studies, such as [33] and [34], to determine the solar capacity for base station sites. The output power at time t is given by:

$$P_{PV}(t) = A_{pan} \cdot P^*_{PV} \cdot \eta_{PV} \left(\frac{G(t)}{G^*} \right) \cdot f_T(t), \tag{5}$$

$$f_T(t) = \left[1 + \vartheta \left(T_{amb}(t) + \frac{G(t)}{800}(NOCT - 20^o C) - T^*_{PV} \right) \right],$$

where:
A_{pan} is the area of the PV panels,
P^*_{PV} is the rated output power per unit area of the PV panels under Standard Test Conditions (STC), provided by the manufacturer,
η_{PV} is the energy conversion efficiency of the panels,
G^* is the solar irradiance under STC (typically 1000W/m^2),
$G(t)$ is the solar irradiance at time t,
ϑ is the power temperature coefficient (typically $-3 \cdot 10^{-3}(1/^\circ\text{C})$ for mono and polycrystalline silicon [35]),
T^*_{PV} is the panel temperature at STC (typically 25°C),
T_{amb} is the ambient temperature, and
$NOCT$ is the nominal operating cell temperature (typically 45°C, as per [32]).

Piezoelectric energy harvesters generate power from mechanical vibrations in the environment. These flexible devices can provide sufficient energy to meet the needs of IoT nodes [36], as mechanical vibrations are commonly present. For a mechanical energy harvester (MEH) operating at resonance, the power output is given by [37]:

$$P_{res} = 4\pi^3 \cdot m_i \cdot f^3_{res} \cdot Z_{max} \cdot Y_0 \tag{6}$$

Where:

m_i is the inertial mass of the harvester, Z_{max} is the maximum displacement, f_{res} is the resonance frequency, and Y_0 is the amplitude of the source motion.

Since renewable energy sources are intermittent, meaning energy availability depends on environmental conditions (e.g., sunlight, wind, RF radiation, vibration), the energy harvesting process can also be modelled as a stochastic process. For simplicity, we assume the arrival times of energy packets follow a Poisson process with the rate λ_H [38, 39]. Over the interval $[0, T]$, the mean energy harvesting rate is:

$$\lambda_H = \frac{1}{\epsilon T} \int_0^T P_H(\tau), d\tau. \tag{7}$$

where $P_H(t)$ represents the harvested energy profile. When energy production exceeds the node's power demand, the surplus is stored in the battery for later use. In this case, the energy packet delivery process from the battery is also assumed to follow a Poisson process with mean rate $\lambda = \lambda_H - \mu$.

The choice of renewable energy sources depends on the IoT application. If a single energy source is insufficient, hybrid energy harvesting systems can be employed, although they may increase the size, weight, and cost of the node. Thus, designing an energy harvesting system involves trade-offs between reliability, mobility, size, weight, and cost. Accurate energy consumption and harvesting models are essential for optimising the energy storage capacity and extending the lifetime of IoT nodes. Therefore, Energy consumption and harvesting models are crucial for sizing the energy storage capacity and determining the lifetime of IoT nodes. In the next chapter, we will discuss the modelling of energy storage systems.

2.3. The energy packet model of the energy storage system

The first step in discretising or quantising energy into energy packets is to determine the quantisation step, which, in our case, corresponds to the size of the energy packet. We define an energy packet (measured in mWh or mAh) as a pulse of power or current lasting for a specified time duration.

Assuming that energy is consumed primarily during active periods—when the node wakes up to perform sensing, computing, or communication—and that the energy consumed during deep sleep periods is negligible, the size of the energy packet can be expressed as:

$$E_p = P_{\text{act}} \cdot t_{\text{act}}$$

where P_{act} is the power consumed during active periods, and t_{act} is the duration of activity.

Although the quantisation step can be set to any arbitrary value, it must remain consistent throughout the quantisation of energy harvesting, consumption, and storage processes.

Let C_B (measured in mWh) denote the capacity of the energy storage system (ESS), which may be a battery or a supercapacitor. The capacity of the ESS in terms of energy packets is given by

$$B = \frac{C_B}{E_p}$$

meaning the ESS can store up to B energy packets. Consequently, the energy states of the ESS are represented as $\{0, 1, 2, \ldots, B\}$. We assume that the node remains dormant and only activates when triggered by a random event, such as fluid leakage in a pipeline monitoring system. Thus, we can assume that the energy consumption process is exponentially distributed. This assumption may not be exact for some other IoT applications, but it can be used as a first-order approximation, making the analysis tractable.

Consider an energy storage system (e.g., a battery, capacitor, or supercapacitor) in an IoT sensor/actuator node. We assume that energy is delivered, stored, and consumed in discrete units called energy packets. This assumption enables the use of queueing models, where customers represent energy packets, and the packet however time corresponds to the service time.

The battery's energy content is modelled using an M/M(n)/1/B queueing system. In Kendall's notation [40], this represents a system with exponentially distributed interarrival and service times, a single server, and a finite capacity limited to B energy packets. The notation M(n) emphasises that the exponential service time distribution has a state-dependent parameter.

Energy delivery follows a Poisson process, meaning that the interarrival times of energy packets are exponentially distributed with rate λ. The time required to consume an energy packet is also exponentially distributed, with rate $\mu(n)$, where n denotes the current number of energy packets in storage.

In a more general Markovian model, the assumption of purely exponential distributions can be relaxed by incorporating phase-type distributions. This allows for a more accurate approximation of real-world distributions. However, this extension increases the number of model states, as each exponentially distributed state is further subdivided into multiple states corresponding to different phases of the chosen distribution.

The service rate $\mu(n)$, defined as the inverse of the average service time, is given by:

$$\mu(n) = \mu_i + \theta(n). \tag{8}$$

Here, μ_i represents the baseline energy consumption rate, while $\theta(n)$ accounts for the state-dependent energy leakage.

The consumption rate may vary depending on the different operational modes of the powered device. For example, when the stored energy exceeds a threshold K ($n > K$), the system operates in normal mode with $\mu_i = \mu_1$. Conversely, if the energy level drops below K ($n \leq K$), the device switches to an energy-saving mode with $\mu_i = \mu_2$.

We consider three different forms of the leakage function $\theta(n)$:

- **Linear Leakage**, proportional to the number of packets in the ESS [2, 26]:

$$\vartheta(n) = \begin{cases} 0, & 0 < n \leq 1, \\ (n-1)\xi, & n \geq 1. \end{cases} \tag{9}$$

- **Exponential Leakage**, typically observed in supercapacitors [22]:

$$\vartheta(n) = \alpha e^{\xi(n-1}, \quad n \geq 1. \tag{10}$$

- **Constant Leakage**, where leakage remains fixed regardless of stored energy [1]:

$$\vartheta(n) = \delta\xi. \tag{11}$$

This modelling framework comprehensively represents energy storage dynamics in IoT devices, enabling precise analysis of performance under various operational conditions.

We model the dynamic changes in the number of energy packets in the energy storage system (ESS) as an $M/M(n)/1/B$ Markovian queueing process

$\{N(t) \mid t \geq 0\}$, where $p(n,t) = \Pr\{N(t) = n\}$ represents the probability of having n energy packets in the ESS at time t. A set of first-order differential equations describes the dynamics of the system, e.g. [41]:

$$\begin{aligned}
\frac{dp(0,t)}{dt} &= -\lambda p(0,t) + \mu(1)p(1,t), \\
\frac{dp(n,t)}{dt} &= -(\lambda + \mu(n))p(n,t) + \lambda p(n-1,t) \\
&\quad +\mu(n+1)p(n+1,t), n = 1, \ldots B-1, \\
\frac{dp(B,t)}{dt} &= \lambda p(B-1,t) - \mu(B)p(B,t). \qquad (12)
\end{aligned}$$

The *steady-state* solution of the above model can be easily obtained as for $t -> \infty$ differential equations become algebraic ones and, [41]

$$p(n) = p(0)\,\frac{\lambda^n}{\mu(1)\ \cdots\ \mu(n)}\,, \quad n = 1, \ldots B \qquad (13)$$

and taking normalisation $\sum_{n=0}^{B} p(n) = 1$,

$$p(0) = \frac{1}{1 + \sum_{n=1}^{B} \{\lambda^n / \prod_{i=1}^{n} \mu(i)\}}\,.$$

3. Evaluation of the energy performance of the node

3.1. Steady-state energy performance analysis

For analytical tractability, we consider a simplified scenario where the leakage rate is linear, and the system has a single energy threshold, below which the node transitions into an energy-efficient mode. The steady-state solution of the system in (12) is derived under these conditions by setting $\frac{dp(n,t)}{dt} = 0$ for all n.

The steady-state probabilities, $p(n)$, can be expressed recursively from the linear system of steady-state equations as follows:

$$p(n) = \left(\frac{\lambda}{\mu_i + (n-1)\xi}\right) p(n-1) \qquad (14)$$

where

$$\mu_i = \begin{cases} \mu_1, & 1 \leq n \leq K-1 \\ \mu_2, & K \leq n \leq B-1 \end{cases}$$

For $n = B$, :

$$p(B) = \frac{\lambda}{\mu_2 + (B-1)\xi} p(B-1).$$

and having regard to normalisation we obtain the probability $p(B)$ which is is a key energy performance metric. It represents the likelihood that the energy

storage system (ESS) reaches its full capacity. When this occurs, any additional energy packets delivered to the ESS are wasted. Therefore, $p(B)$ can be interpreted as the probability of energy waste, providing insight into the system's efficiency in utilising harvested energy.

The probability $p(0)$ is another crucial energy performance metric, representing the likelihood that the energy storage system (ESS) is completely depleted of energy packets, causing the system to shut down. This probability can also be interpreted as the service outage probability, indicating the risk of system unavailability due to insufficient stored energy. This formulation analytically characterises the steady-state probabilities, accounting for both energy leakage effects and state-dependent transitions. Therefore, the steady-state probability $P(n)$ is given by:

$$p(n) = \begin{cases} \prod_{r=1}^{n} \left(\frac{\lambda}{\mu_1 + (r-1)\xi} \right) p(0), & 1 \leq n < K, \\ \left(\prod_{r=1}^{K-1} \frac{\lambda}{\mu_1 + (r-1)\xi} \right) \left(\prod_{l=K}^{n} \frac{\lambda}{\mu_2 + (l-1)\xi} \right) p(0), & K \leq n \leq B. \end{cases}$$

Using the normalisation condition:

$$\sum_{n=0}^{N} p(n) = 1,$$

we obtain $p(0)$ as:

$$p(0) = \left[1 + \sum_{n=1}^{K-1} \prod_{r=1}^{n} \frac{\lambda}{\mu_1 + (r-1)\xi} + \sum_{n=K}^{B} \prod_{r=1}^{K-1} \frac{\lambda}{\mu_1 + (r-1)\xi} \prod_{l=K}^{n} \frac{\lambda}{\mu_2 + (l-1)\xi} \right]^{-1}.$$

Fig. 3 illustrates the steady-state distribution $p(n)$ of energy packets in the energy storage system. As in all examples, the energy storage system (ESS) has a capacity of $B = 100$ energy packets.

The system operates in two modes depending on the storage system's energy level, with different consumption rates:

- $\mu_2 = 5$ when $n > K$
- $\mu_1 = 3$ when $n \leq K$

The energy leakage follows a linear model with coefficient ξ, while incoming packet arrivals occur at an intensity of $\lambda = 12$. The figure demonstrates the impact of ξ on the energy distribution: as leakage increases, the stored energy decreases accordingly. The results presented in table 1 indicate that as ξ increases, both the mean and variance decrease. This suggests that a higher ξ

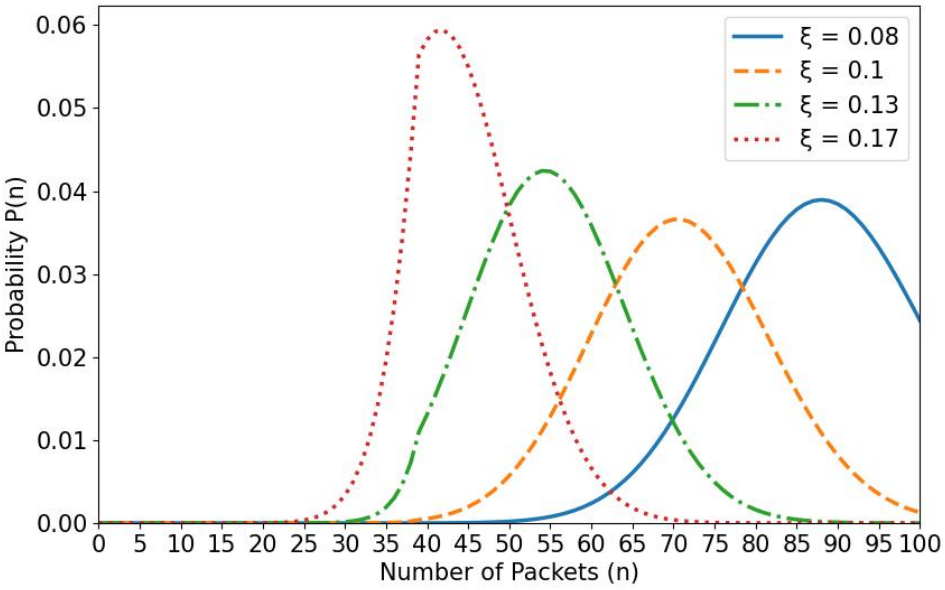

Figure 3: Influence of ξ on the probability $p(n)$ of having n energy packets in the ESS, for $\lambda = 12$, $\mu_2 = 5$, $\mu_1 = 3$, $K = 40$, $B = 100$

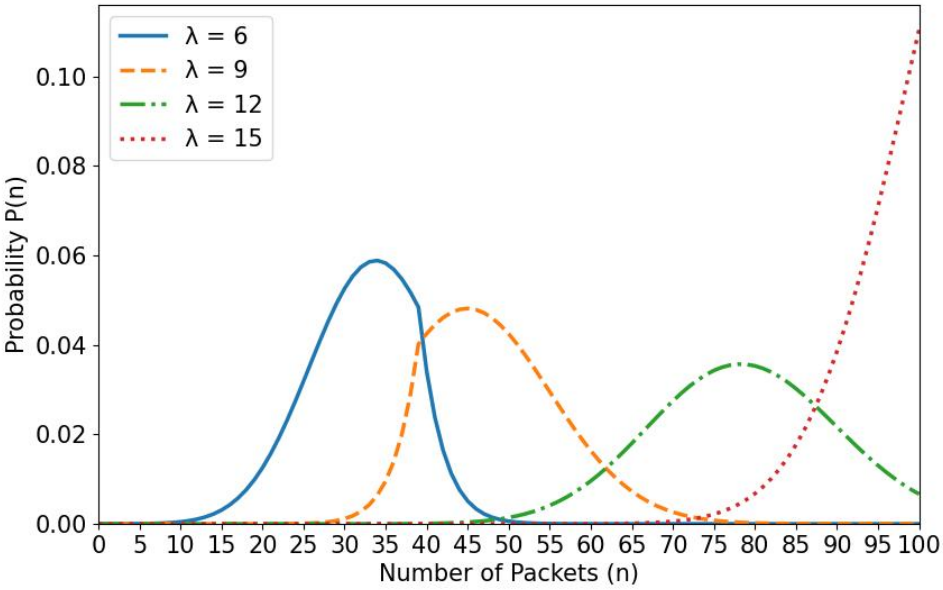

Figure 4: Influence of λ on the probability, $p(n)$ of having n energy packets in the ESS, for $\xi = 0.09$, $\mu_2 = 5$, $\mu_1 = 3$, $K = 40$, $B = 100$

Table 1: The mean and variance of the number of EPs in the energy storage system for different values of ξ.

ξ	Mean	Variance
0.08	84.84061	90.85228
0.1	70.86492	114.82898
0.13	55.31960	83.77020
0.17	44.84754	48.01065

leads to a lower number of energy packets stored in the ESS. That is, the higher the energy leakage rate, the lower the number of EPs stored in the ESS.

Fig. 4 illustrates the impact of increasing the mean energy delivery rate λ on the steady-state distribution of the number of energy packets in the storage system. Similarly, for varying λ, increasing the arrival rate of energy packets initially raises both the mean and variance, indicating a higher mean number of energy packets in the ESS and greater variability. However, at $\lambda = 15$, the variance significantly drops, suggesting that the system may be reaching a saturation point where additional arrivals of energy packets do not substantially increase variability.

Table 2: The mean and variance of the number of EPs in the energy storage system for different values of λ.

λ	Mean	Variance
6	31.93525	42.43200
9	48.35173	66.78113
12	77.89332	112.73011
15	93.69160	32.04958

Figs. 5 and 6 illustrate the steady-state probability $p(0)$, which represents the likelihood that the battery is empty. The dependence of $p(0)$ on the consumption rate μ_1 and the arrival intensity λ is analyzed. As expected, $p(0)$ decreases as λ increases, with the decline occurring more rapidly for lower consumption rates μ_1 and smaller leakage rates ξ.

Fig. 7 further explores the variation of the probability of an empty battery with respect to the leakage rate ξ and input intensity λ. As in the previous analysis, a linear leakage model is assumed, with ξ varying within the range $[0, 1]$. The consumption rates are fixed at $\mu_2 = 5$ and $\mu_1 = 3$. The results confirm that an increase in ξ leads to a higher probability of battery depletion, while an increase in λ reduces this probability.

3.2. Transient-state energy performance analysis

We analyse the transient-state energy performance of the ESS with and without energy thresholds. While steady-state analysis assumes constant mean rates for energy packet delivery to and consumption from the ESS, the mean

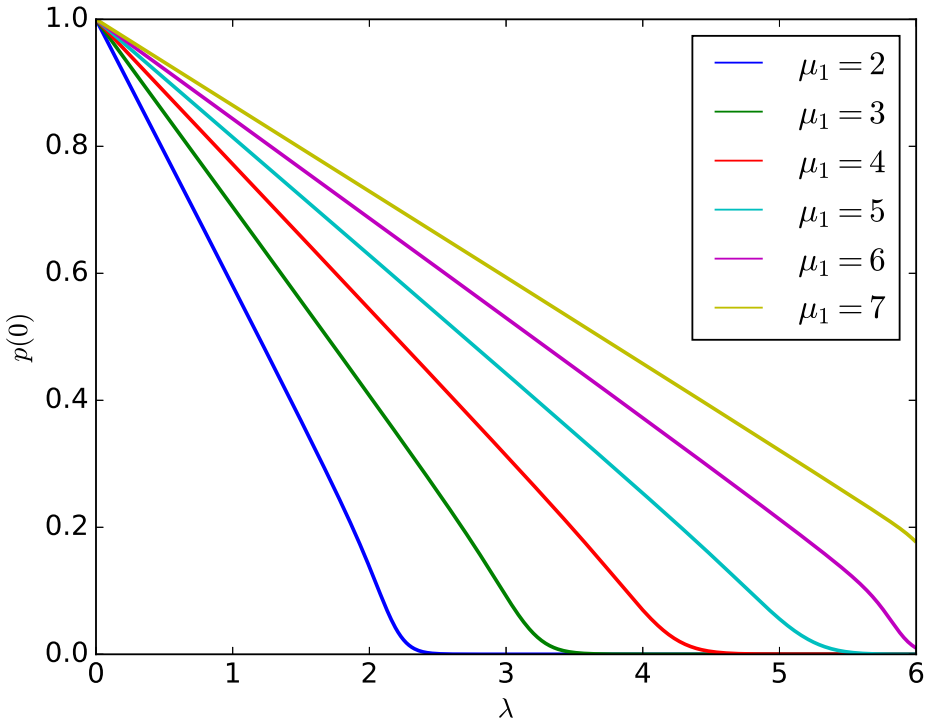

Figure 5: Influence of μ_1 on the probability, $p(0)$ of depleting all of the energy packets stored in the ESS, for $\xi = 0.05$, $\mu_2 = 5$, $K = 40$, $B = 100$

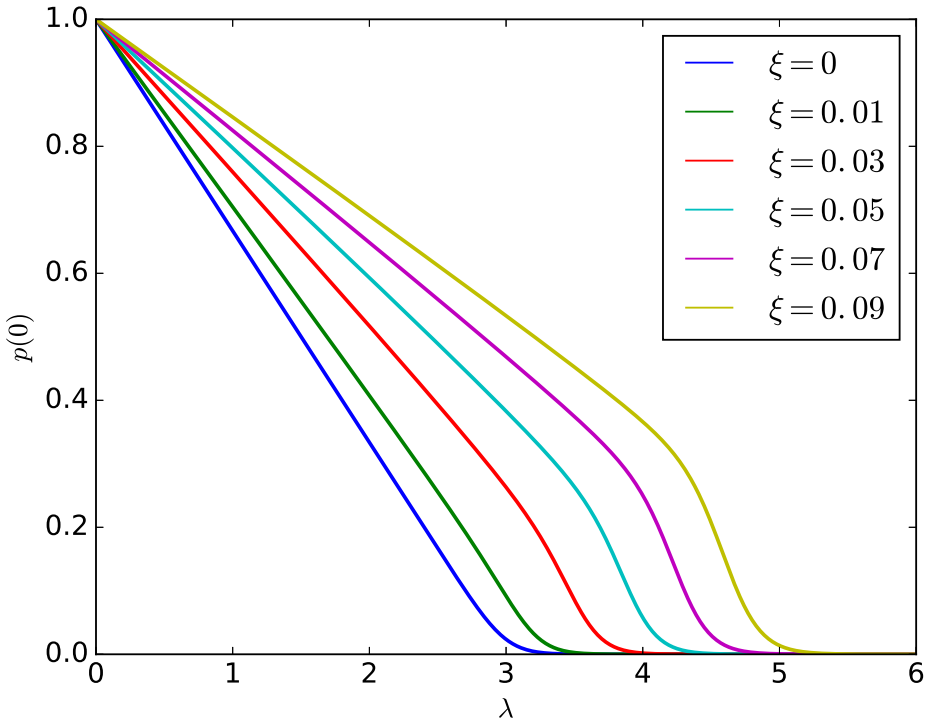

Figure 6: Influence of ξ on the probability, $p(0)$ of depleting all of the energy packets stored in the ESS, for $\mu_2 = 5$, $\mu_1 = 3$, $K = 40$, $B = 100$

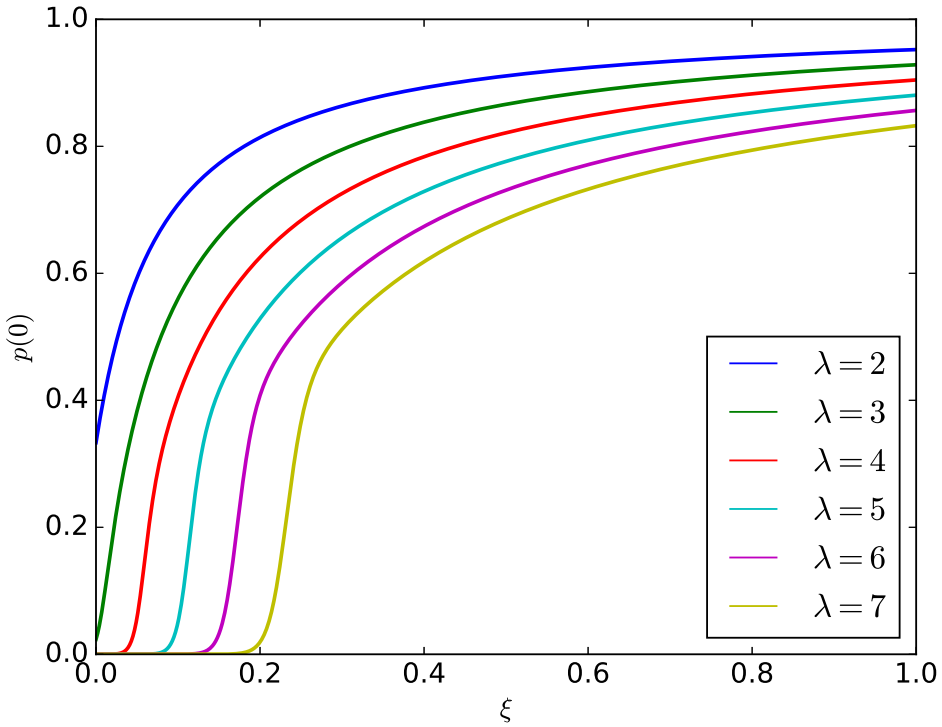

Figure 7: Influence of λ on the probability, $p(0)$ of depleting all of the energy packets stored in the ESS, for $\mu_2 = 5$, $\mu_1 = 3$, $K = 40$, $B = 100$

number of harvested energy packets can fluctuate over time. We evaluate the impact of parameters such as energy leakage rate, energy harvesting rate, and the energy consumption rate on the mean number of energy packets present in the ESS at time t. The expected value of the number of energy packets in the ESS at time t, denoted as $E[N(t)]$ is the weighted sum of the probabilities of being at each state n, i.e.,

$$E[N(t)] = \sum_{n=0}^{B} np(n,t).$$

The *transient solution* of (12) is more intricate. It can be obtained using the Laplace transform, which converts the system's differential equations into algebraic equations in the Laplace domain. This transformation allows for an analytical solution. However, this solution must be inverted numerically. Alternatively, a direct numerical approach can be used, as demonstrated here with our solver. Many other solvers may be helpful.

We consider a periodically varying harvesting rate, λ, that alternates between day and night cycles of equal duration. Specifically, during the daytime of each 24-hour cycle, energy packets are delivered to the ESS at a rate of λ, whereas during the nighttime, the harvesting rate drops to zero ($\lambda = 0$). Given that both periods last for 12 hours, λ undergoes a step change at the end of each half-cycle.

At each time step, we compute the transient state probabilities, which are then used to determine the transient mean number of energy packets in the ESS using Equation (3.2). The probability distribution at the end of each day or night period serves as the initial condition for the subsequent period, ensuring a continuous update of the system dynamics.

The impact of the energy leakage parameter, ξ, on the evolution of the mean number of energy packets stored in the ESS is illustrated in Figs. 8 and 9. We assume that the process begins at $t = 0$ during the night period ($\lambda = 0$). It can be observed that the depletion rate of energy packets during the first night's period in the 24-hour cycle is particularly steep. This sharp decline is primarily due to energy leakage, as the leakage rate is proportional to the number of energy packets stored in the ESS. The sharp decline is also due to the high energy consumption rate $\mu_2 = 5$ because initially, the number of stored energy packets is above the defined threshold of $K = 0.4B = 40$ energy packets. When the number of stored energy packets is below 40, the energy consumption rate changes to $\mu_1 = 3$ (the node is forced into an energy-saving regime). We consider three cases with different values of the energy leakage parameter: $\xi = 0$ (no energy leakage), $\xi = 0.01$, and $\xi = 0.05$.

Fig. 8 shows that as the energy leakage parameter ξ increases, the rate of depletion of stored energy packets significantly rises. This occurs because a higher ξ leads to an increased energy leakage rate, accelerating the depletion of energy packets in the ESS over time. A similar trend is observed in Fig. 9, where all parameters remain the same as in Fig. 8, except for the energy delivery rate during the day, which is increased to $\lambda = 10$. The impact of the

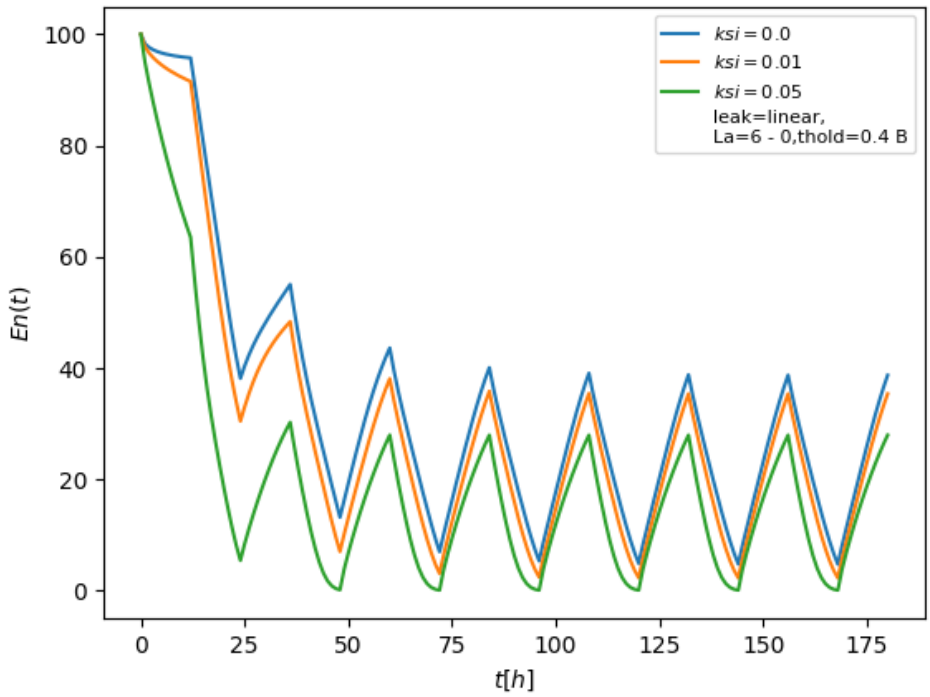

Figure 8: The influence of ξ on the evolution of $E[N(t)]$ for several day and night cycles considering: $\lambda = 6$ (during the day) and $\lambda = 0$) (during the night), $\mu_2 = 5$, $\mu_1 = 3$, $K = 40$, $B = 100$, linear leakage, $\xi = \{0, 0.01, 0.05\}$

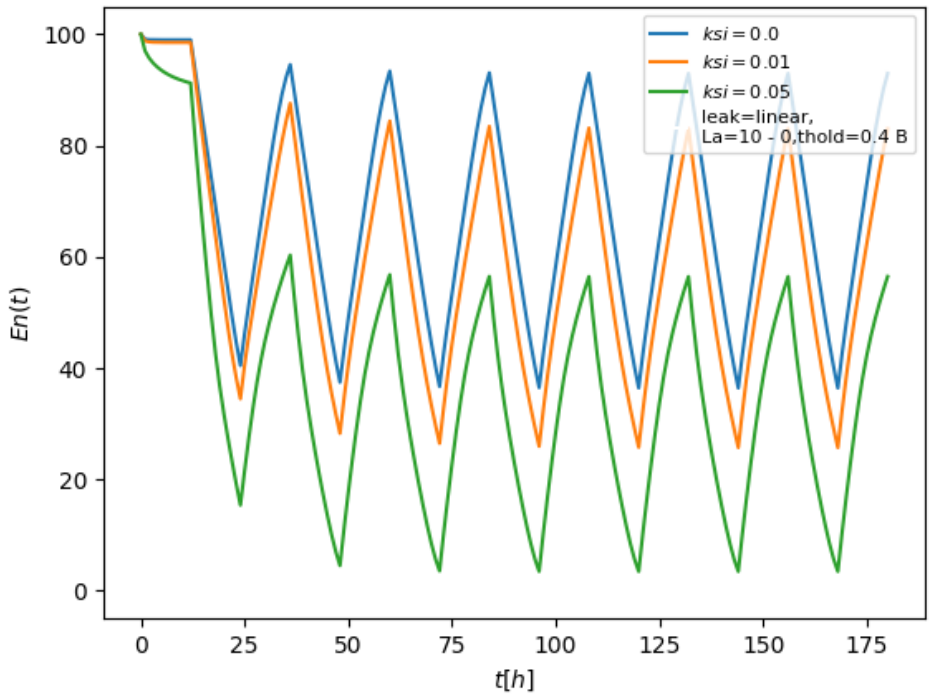

Figure 9: The influence of ξ on the evolution of $E[N(t)]$ for several day and night cycles considering: $\lambda = 10$ (during the day) and $\lambda = 0$) (during the night), $\mu_2 = 5$, $\mu_1 = 3$, $K = 40$, $B = 100$, linear leakage, $\xi = \{0, 0.01, 0.05\}$

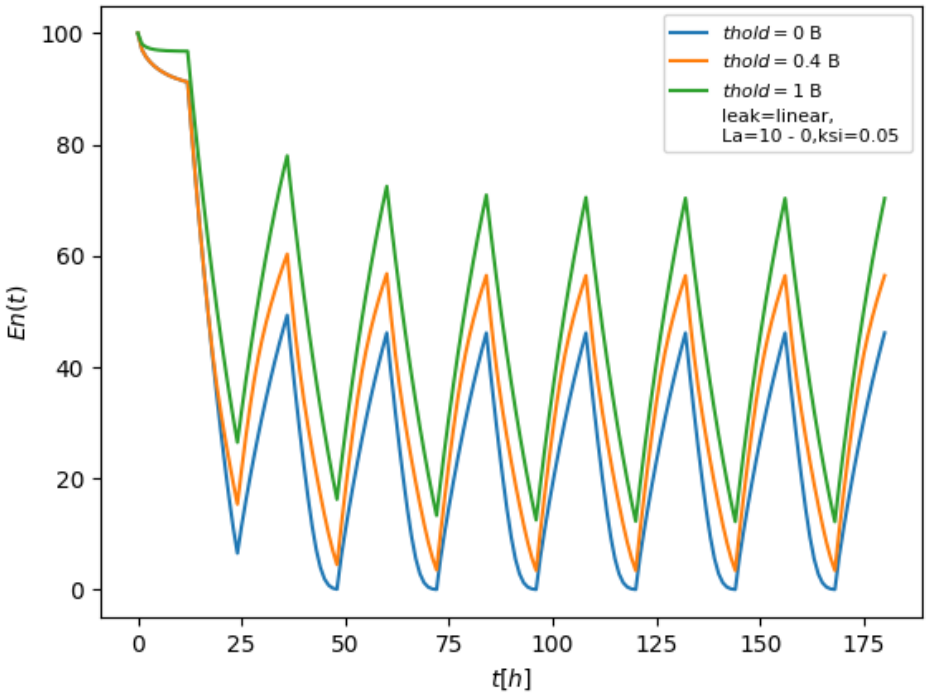

Figure 10: The influence of K on the evolution of $E[N(t)]$ for several day and night cycles considering: $\lambda = 6$ (during the day) and $\lambda = 0$) (during the night), $\mu_2 = 5$, $\mu_1 = 3$, $\xi = 0.05$, $B = 100$, linear leakage, $K = \{0, 40, 100\}$

energy leakage parameter is more pronounced in this case, as a higher energy delivery rate (λ) results in a larger number of stored energy packets during the day, subsequently leading to a higher rate of energy leakage at night.

Additionally, it can be observed that for $\lambda = 10$, a sufficient number of energy packets remain in the ESS at the end of each night period, preventing complete depletion. An important takeaway from these results is that the energy harvester should be sized appropriately to ensure that the mean number of energy packets remaining in the ESS at the end of each night period is not zero. In other words, complete depletion of stored energy packets should be avoided to maintain system reliability.

Figs. 10–12 illustrate the impact of the energy threshold K, below which the energy consumption rate is reduced from $\mu_2 = 5$ to $\mu_1 = 3$. Specifically, when the number of stored energy packets exceeds the defined threshold, the energy consumption rate remains at $\mu_2 = 5$, which is reflected in the steep decline in stored energy due to the combined effects of high energy consumption and energy leakage. However, once the number of energy packets falls below K, the

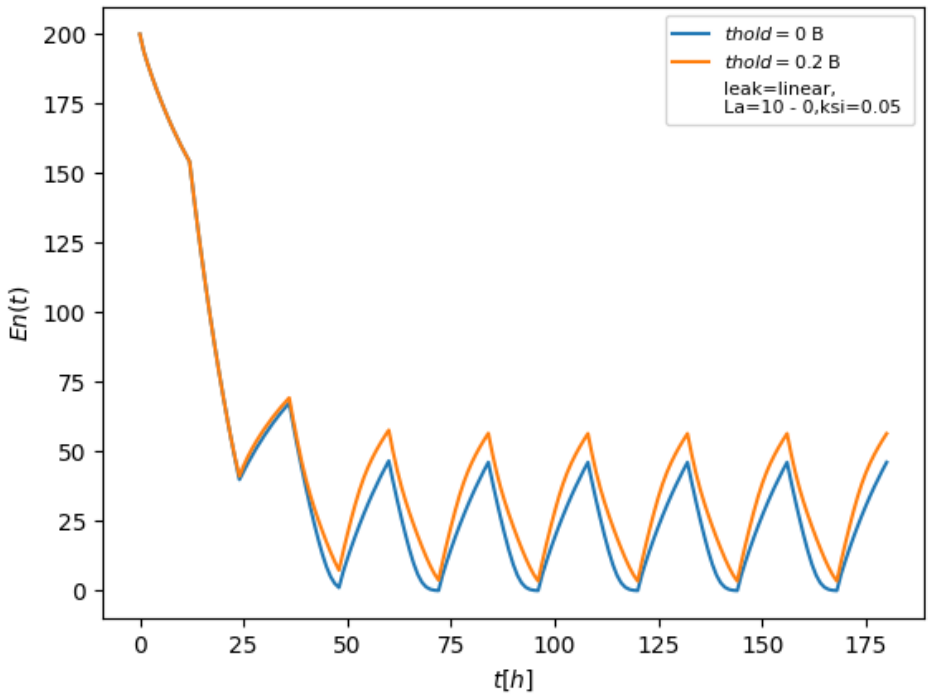

Figure 11: The influence of K on the evolution of $E[N(t)]$ for several day and night cycles considering: $\lambda = 10$ (during the day) and $\lambda = 0$) (during the night), $\mu_2 = 5$, $\mu_1 = 3$, $\xi = 0.05$, $B = 200$, linear leakage, $K = \{0, 40\}$

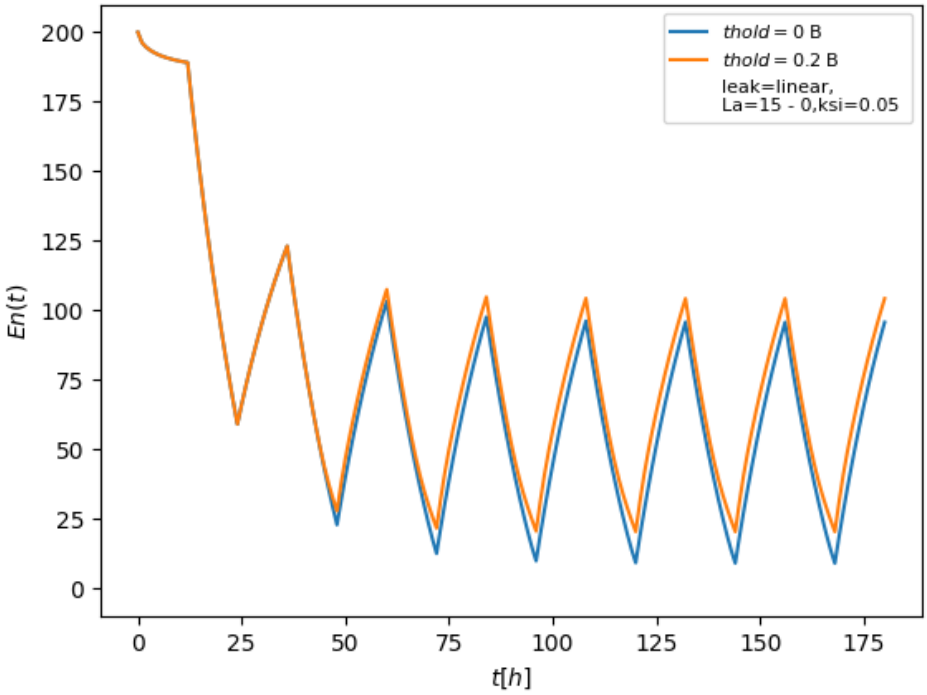

Figure 12: The influence of K on the evolution of $E[N(t)]$ for several day and night cycles considering: $\lambda = 15$ (during the day) and $\lambda = 0$) (during the night), $\mu_2 = 5$, $\mu_1 = 3$, $\xi = 0.05$, $B = 200$, linear leakage, $K = \{0, 40\}$

energy consumption rate is reduced to $\mu_1 = 3$, leading to a slower depletion rate due to both reduced consumption and lower energy leakage.

In Fig. 10, we analyze three scenarios: (i) $K = 100$, where the energy consumption is maintained at an optimal level of $\mu = \mu_1 = 3$; (ii) $K = 0.4B = 40$; and (iii) $K = 0$, where the high energy consumption rate remains constant at $\mu = \mu_2 = 5$. It can be observed that as K decreases, the mean number of stored energy packets at time t also decreases. This occurs because an earlier transition into the energy-saving regime (i.e., switching to a lower energy consumption rate) slows down the depletion of stored energy.

Fig. 11 further examines two low-threshold cases: $K = 0$ and $K = 0.2B = 40$ given that $B = 200$. Since these thresholds are relatively small, the node operates in the high energy consumption regime ($\mu_2 = 5$) for most of the time, causing a rapid depletion of stored energy. To mitigate this, the energy delivery rate to the ESS can be increased, as demonstrated in Fig. 12.

In Fig. 11, it is evident that an energy delivery rate of $\lambda = 10$ during the day is insufficient to accumulate enough energy to sustain the node throughout the night period. To address this, the mean delivery rate of energy packets during the day is increased from $\lambda = 10$ to $\lambda = 15$, and the storage capacity of the ESS is expanded from $B = 100$ to $B = 200$ energy packets. This highlights that the adverse effects of energy leakage can be mitigated either by configuring higher energy-saving thresholds or by scaling up the energy harvesting system.

3.3. Evaluation of the impact of energy leakage on the lifetime of the node

We investigate the impact of energy leakage parameters and energy leakage functions (linear, exponential, or constant) on the device's lifetime. The device's lifetime is defined as the time required to deplete all the stored energy packets[19, 17]. We model the device's lifetime as the first passage time of the M/M(n)/1/B queueing model, where the process starts from any initial state and is absorbed at $n = 0$. The density of the first passage time denoted as $\gamma_{i,0}(t)$, represents the time it takes for the process to go from a starting state $n = i$ to absorption at $n = 0$. This can be numerically computed modifying the M/M(n)/1/B model.

To calculate the first passage time from B to zero in the M/M(n)/1/B model, we treat state zero as an absorbing state. This results in a modification of the system's equations. Specifically, we modify the first equation as follows:

$$\frac{dp(0,t)}{dt} = \mu(1)p(1,t);$$

where $p(1,t)$ is computed for the chain initiated from state B. The intensity of entry into state 0, as represented by the equation above, corresponds to the density of the first passage time from B to 0:

$$\gamma_{B,0}(t) = \mu(1)p(1,t). \tag{15}$$

Similarly, to model the first passage time from 0 to B (i.e., the time required to charge the ESS to full capacity), we treat state B as the absorbing state and

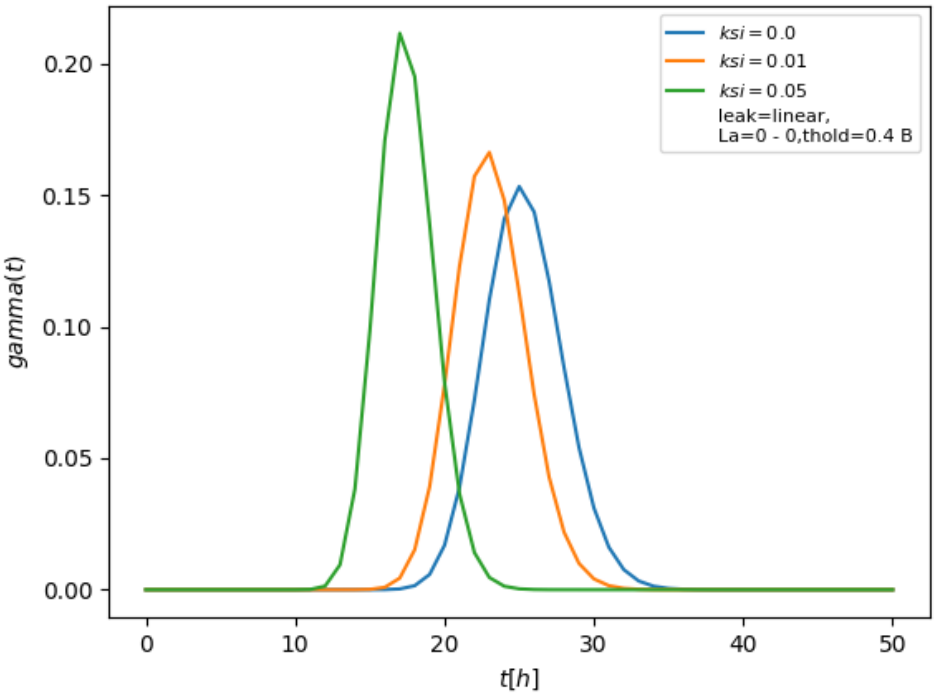

Figure 13: Influence of ξ on the PDF of the life of the node, $\gamma_{B,0}(t)$, for $\lambda = 0$ (the energy harvester is off for several hours), $\mu_1 = 3$ $\mu_2 = 5$, $K = 40$, $B = 100$.

compute $p(B-1,t)\lambda$ for the chain initiated from state B. The corresponding first passage time density is:

$$\gamma_{0,B}(t) = \lambda p(B-1,t). \tag{16}$$

Both performance metrics, $\gamma_{B,0}$ (the node's lifetime) and $\gamma_{0,B}$ (the charging time), can be obtained numerically using a Markov solver to estimate the lifetime of an IoT node.

One of the key performance metrics considered is the probability density function (PDF) of the node's lifetime, defined as the time required to deplete all stored energy packets. This PDF is estimated using Equation (15). The system of equations in Equation (12) is solved numerically. Since the process is absorbed upon reaching state $n = 0$, the first passage time from state $n = B$ to $n = 0$ (i.e., the node's lifetime distribution) corresponds to the rate at which the process enters state $n = 0$, given by $\mu_1 p(1,t)$.

Energy harvesting sources are prone to failure; thus, solar-powered green IoT nodes must be designed to withstand such failures. In this scenario, we

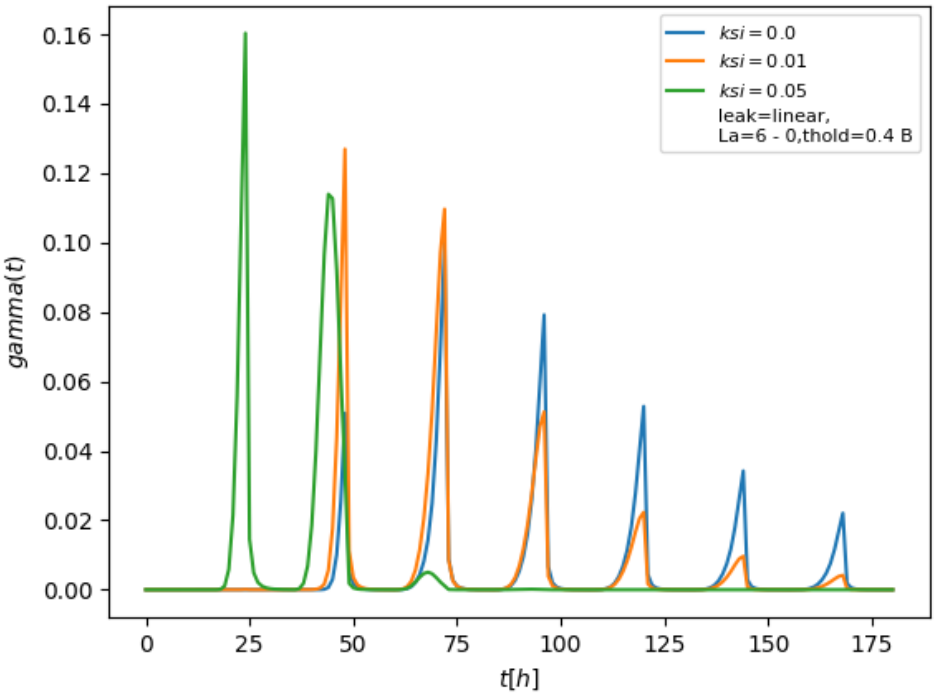

Figure 14: Influence of ξ on the PDF of the life of the node, $\gamma_{B,0}(t)$, for $\lambda = 6$ (during the day period) and $\lambda = 0$ (during the night period), $\mu_1 = 3$ $\mu_2 = 5$, $K = 40$, $B = 100$.

estimate the autonomy of the node, defined as its lifetime when no external energy sources are available (i.e., $\lambda = 0$). This analysis determines how long the node can function solely on its initially stored energy.

Figure 13 illustrates the impact of the leakage parameter ξ on the node's autonomy. We consider three cases: (i) $\xi = 0$ (no energy leakage), (ii) $\xi = 0.01$ (yellow line), and (iii) $\xi = 0.05$ (green line), assuming a linear energy leakage model. As ξ increases, the PDF of the depletion time shifts leftward, indicating a shorter lifetime. This occurs because a higher leakage parameter increases the mean energy dissipation rate, thereby reducing the expected time before all stored energy is depleted.

In Figure 14, we estimate the lifetime of a solar-powered green IoT node. As in Figure 13, we assume that the energy leakage rate is proportional to the energy stored in the energy storage system (ESS). We consider three leakage scenarios: (i) $\xi = 0$ (blue line), (ii) $\xi = 0.01$ (yellow line), and (iii) $\xi = 0.05$ (green line).

The spikes in the probability density function (PDF) indicate the impact

of energy during the day ($\lambda = 6$), followed by a sharp decline at night when no energy is harvested ($\lambda = 0$). Over time, these peaks diminish, with the highest leakage case ($\xi = 0.05$) decreasing the fastest, followed by $\xi = 0.01$. This highlights the impact of energy leakage: in an ideal ESS ($\xi = 0$), stored energy depletes much more slowly than in a non-ideal ESS with leakage.

3.4. Evaluation of the impact of energy harvesting and management on the service outage probability

Another important performance metric is the transient service outage probability which is the probability $p(0,t)$ that at time t, all the stored energy packets will be depleted. When all the stored energy packets are depleted, the node is shutdown which disrupts the IoT services. It is desirable to size the energy harvesters and energy storage system in such a way as to ensure that the service outage probability is very small.

The service outage probability can be obtained by solving for the transient state probability $p(0,t)$ in the system of differential equations in equation 12. At each time step, $p(0,t)$ is computed and its evolution is tracked over time and then plotted.

Figs. 15 and 16 illustrate the evolution of the service outage probability. To examine the influence of the threshold K on service outage probability, we consider two primary cases: $K = \{0, 40\}$ for $\lambda = 10$ and $K = \{0, 40\}$ for $\lambda = 15$. In both scenarios, the system parameters are fixed as $\mu_2 = 5$, $\mu_1 = 3$, $\xi = 0.05$, and $B = 200$.

The sharp spikes in Fig. 15 occur during the night periods when the ESS is in discharge mode, as energy packets are depleted due to energy leakage and normal consumption without replenishment. Conversely, the troughs correspond to charging periods during the day, where increased energy delivery to the ESS reduces the service outage probability.

For a fixed arrival rate λ (e.g., $\lambda = 10$), the service outage probability decreases as K is lowered from $K = 0.2B = 40$ to $K = 0$. This occurs because, in the latter case, the node remains in the high energy consumption regime ($\mu_2 = 5$), whereas in the former case, it switches to the energy-saving regime ($\mu_1 = 3$) once the threshold $K = 0.2B = 40$ is reached.

The impact of the energy delivery rate λ is also evident, as a moderate increase in λ from 10 to 15 significantly reduces the service outage probability. This highlights the importance of configuring appropriate values for K and λ and reinforces the fact that energy leakage effects can be mitigated by increasing the energy-saving threshold or scaling up the energy harvesting system.

Fig. 16 presents the same results as Fig. 15, but on a logarithmic scale, allowing for better visualization of small values of $p(0,t)$.

3.5. The impact of the energy leakage model on the energy performance metrics

The energy leakage rate model varies across different energy storage systems (ESS). For instance, in some ESS, the leakage rate decreases almost linearly

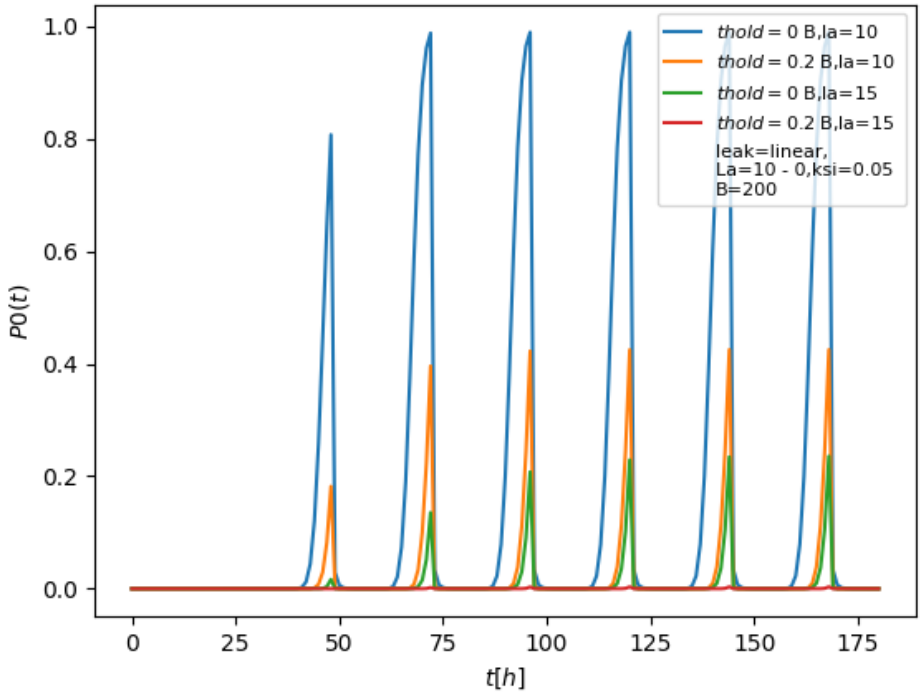

Figure 15: The influence of K and λ on the evolution of $p(0,t)$ (linear scale) for several day and night cycles considering: $\lambda = \{10, 15\}$ (during the day) and $\lambda = 0$) (during the night), $\mu_2 = 5$, $\mu_1 = 3$, $\xi = 0.05$, $B = 200$, linear leakage, $K = \{0, 40\}$.

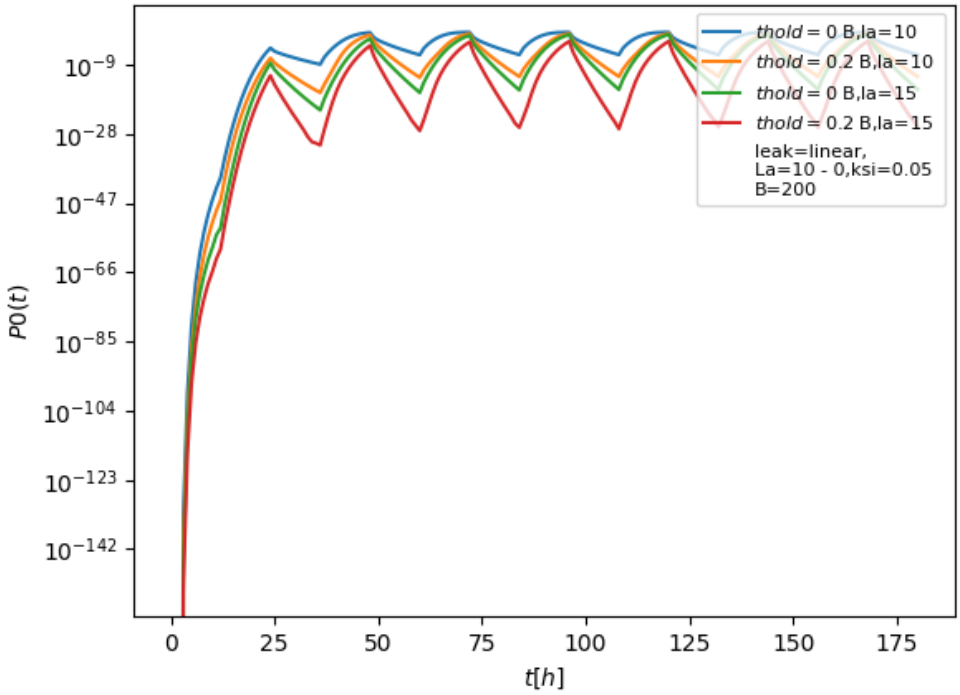

Figure 16: The influence of K and λ on the evolution of $p(0,t)$ (logarithmic scale) for several day and night cycles considering: $\lambda = \{10, 15\}$ (during the day) and $\lambda = 0$) (during the night), $\mu_2 = 5$, $\mu_1 = 3$, $\xi = 0.05$, $B = 200$, linear leakage, $K = \{0, 40\}$.

with the number of stored energy packets, following the model:

$$\vartheta(n) = (n-1)\xi, \quad n \geq 1 \tag{17}$$

as described in [2, 26].

In contrast, certain ESS exhibit a fairly constant energy leakage rate:

$$\vartheta(n) = \delta\xi \tag{18}$$

as reported in [1].

For energy storage systems such as supercapacitors, the leakage rate may vary exponentially with the number of stored energy packets:

$$\vartheta(n) = \alpha e^{\xi(n-1)}, \quad n \geq 1 \tag{19}$$

as shown in [22]. Experimental validation of this relationship can be found in [42, 43, 44].

Given these variations, it is crucial to investigate and compare the impact of different energy leakage models on key energy performance metrics.

The impact of different energy leakage models on key energy performance metrics, namely the service outage probability and the mean number of stored energy packets at time t, is illustrated in Figs. 17–20. The system parameters used for this analysis are: $\lambda = 6$ (during the day) and $\lambda = 0$ (during the night), $\mu_2 = 5$, $\mu_1 = 3$, $\xi = 0.01$, $K = 0.4B = 40$, and $B = 100$. In each case, the corresponding energy leakage rate is incorporated into the system of differential equations in Eq. (12). The system is then solved, and the evolution of $p(0,t)$ and $E[N(t)]$ is tracked as described in the previous subsections.

Fig. 17 shows that the peaks of the exponential energy leakage model (blue curve) are significantly higher than those of the other models. This occurs because, in the exponential leakage model, the leakage rate increases exponentially with the number of stored energy packets, leading to rapid depletion. Consequently, the exponential leakage model performs the worst in terms of energy retention, followed by the linear leakage model (yellow curve), while the constant leakage model (green curve) demonstrates the best performance. The constant leakage model is advantageous because its leakage rate remains fixed and does not depend on the number of stored energy packets.

Fig. 18 presents the same information as Fig. 17, but with a logarithmic scale on the y-axis to highlight low values of $p(0,t)$. A similar trend is observed in Fig. 20, which illustrates the influence of energy leakage models on the evolution of the mean number of stored energy packets, $E[N(t)]$. The mean number of stored energy packets is significantly lower under the exponential leakage model compared to the other models.

Initially, the gap between the exponential leakage model and the other models is substantial, as higher energy levels lead to exponentially higher energy losses. However, as the mean stored energy decreases, the difference between the exponential and linear leakage models becomes less pronounced. Over time, the linear and constant leakage models converge for low values of stored energy

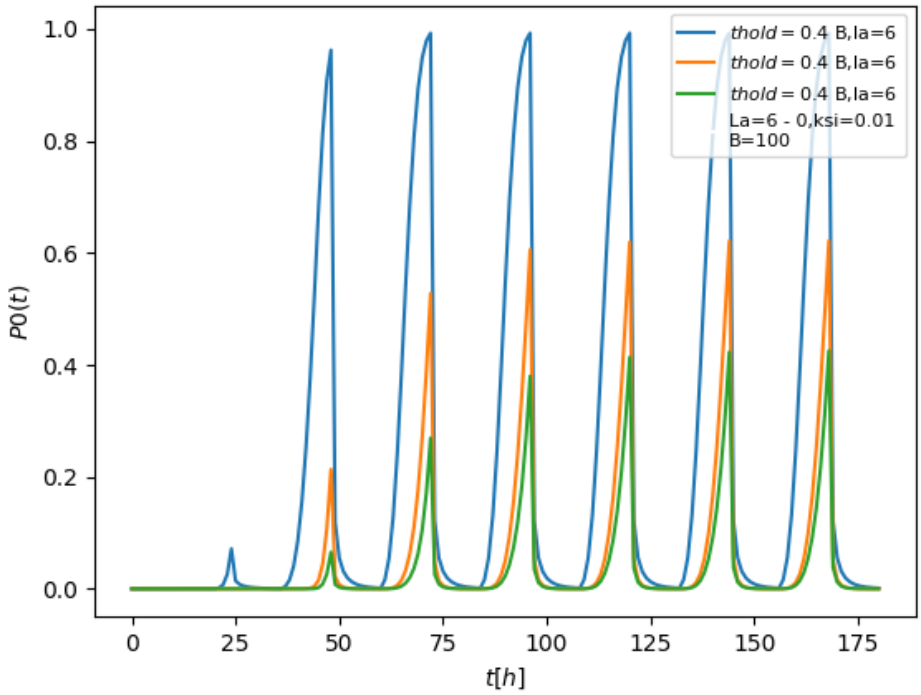

Figure 17: The influence of the energy leakage model (constant leakage rate in green curve, linear leakage rate in yellow curve, and the exponential leakage rate in blue curve) on the evolution of $p(0,t)$ (logarithmic scale) for several day and night cycles considering: $\lambda = 6$ (during the day) and $\lambda = 0$) (during the night), $\mu_2 = 5$, $\mu_1 = 3$, $\xi = 0.01$, $K = 0.4B = 40$, $B = 100$.

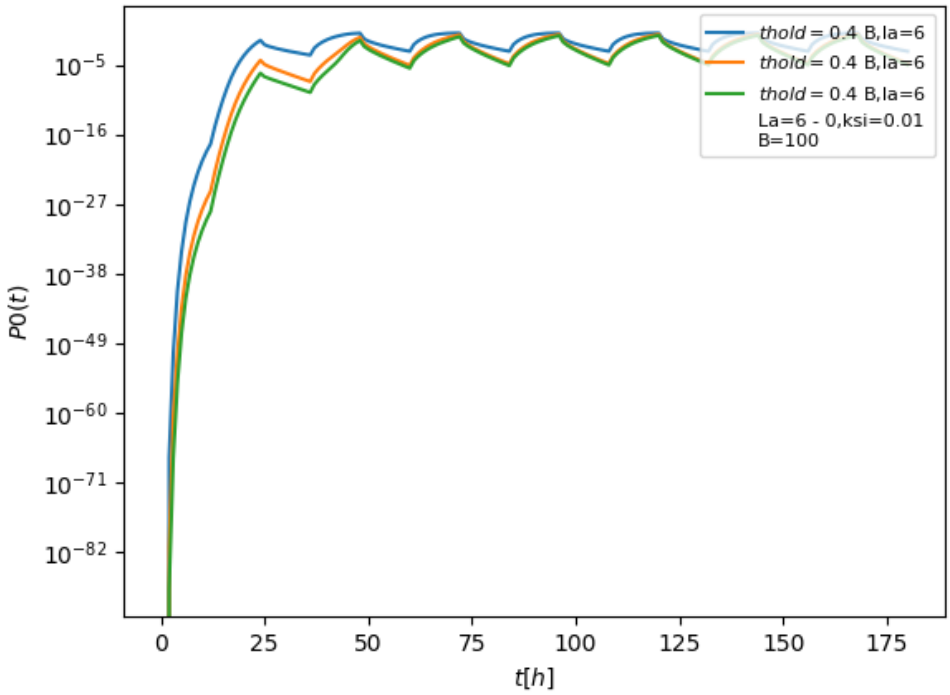

Figure 18: The influence of the energy leakage model (constant leakage rate in green curve, linear leakage rate in yellow curve, and the exponential leakage rate in blue curve) on the evolution of $p(0,t)$ (linear scale) for several day and night cycles considering: $\lambda = 6$ (during the day) and $\lambda = 0$) (during the night), $\mu_2 = 5$, $\mu_1 = 3$, $\xi = 0.01$, $K = 0.4B = 40$, $B = 100$.

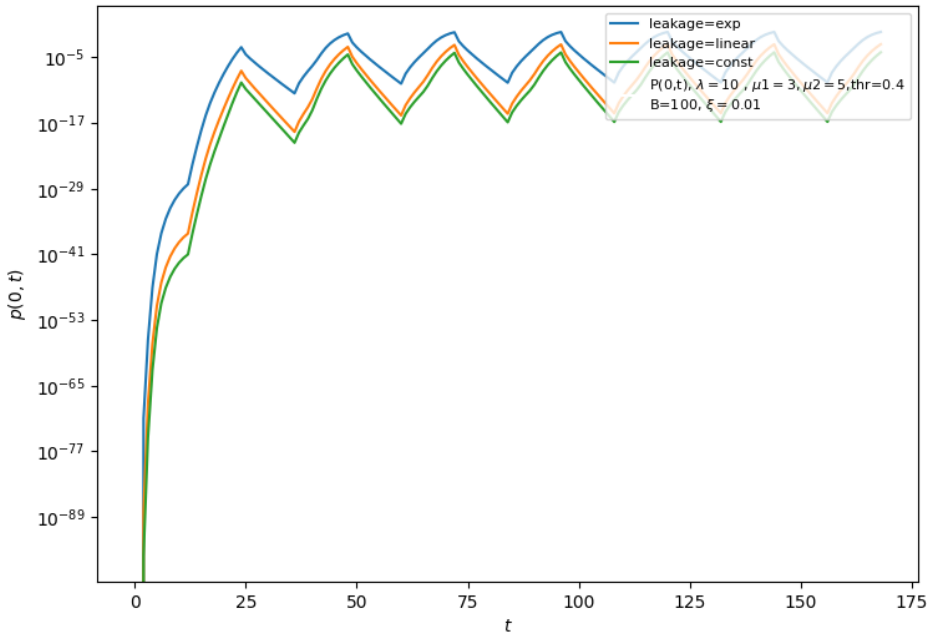

Figure 19: The influence of the energy leakage model (constant leakage rate in green curve, linear leakage rate in yellow curve, and the exponential leakage rate in blue curve) on the evolution of $p(0,t)$ (linear scale) for several day and night cycles considering: $\lambda = 6$ (during the day) and $\lambda = 0$) (during the night), $\mu_2 = 5$, $\mu_1 = 3$, $\xi = 0.01$, $K = 0.4B = 40$, $B = 100$.

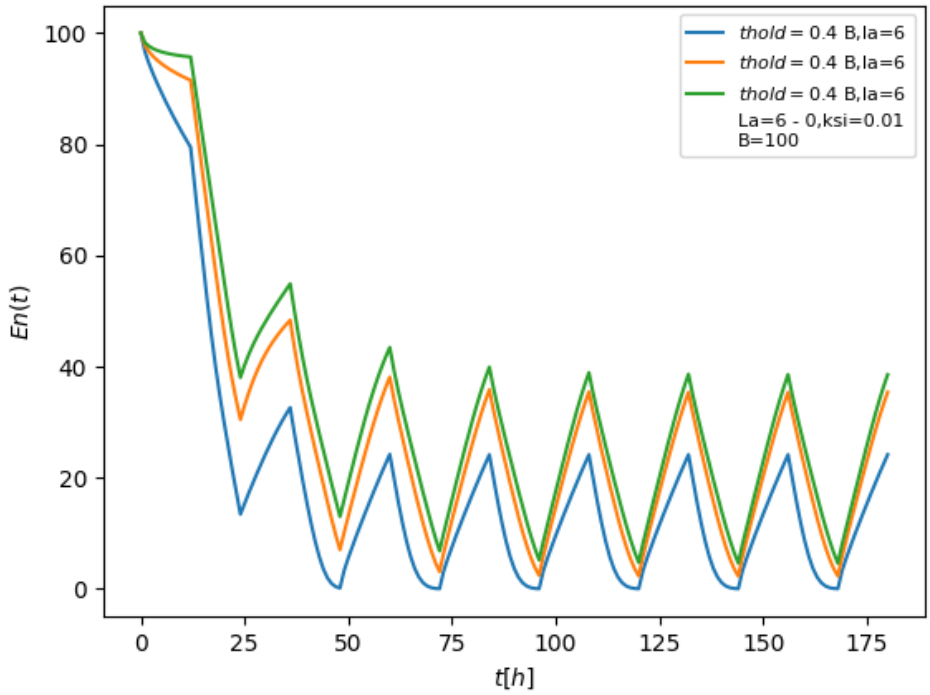

Figure 20: The influence of the energy leakage model (constant leakage rate in green curve, linear leakage rate in yellow curve, and the exponential leakage rate in blue curve) on the evolution of $E[N(t)]$ for several day and night cycles considering: $\lambda = 6$ (during the day) and $\lambda = 0$) (during the night), $\mu_2 = 5$, $\mu_1 = 3$, $\xi = 0.01$, $K = 0.4B = 40$, $B = 100$.

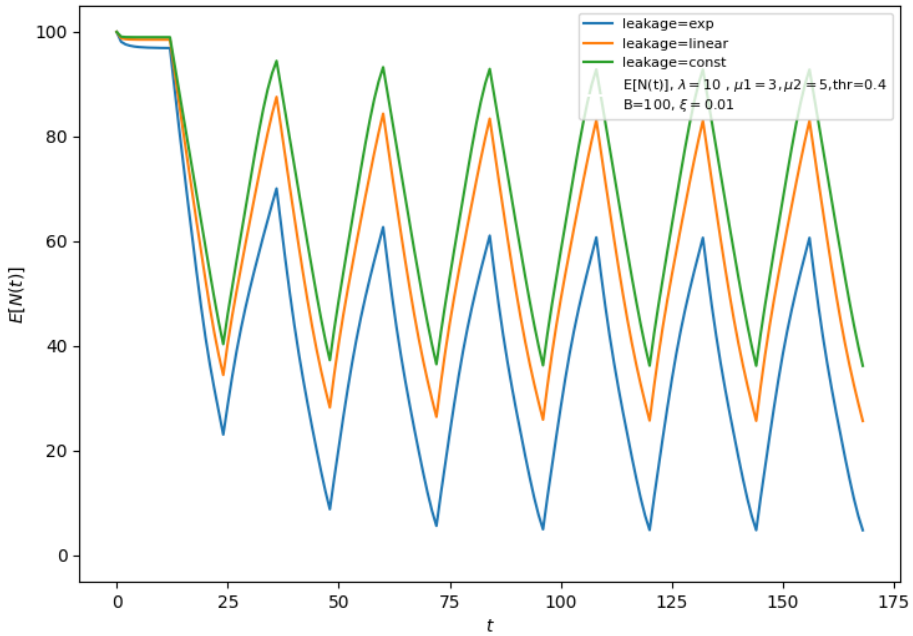

Figure 21: The influence of the energy leakage model (constant leakage rate in green curve, linear leakage rate in yellow curve, and the exponential leakage rate in blue curve) on the evolution of $E[N(t)]$ for several day and night cycles considering: $\lambda = 10$ (during the day) and $\lambda = 0$) (during the night), $\mu_2 = 5$, $\mu_1 = 3$, $\xi = 0.01$, $K = 0.4B = 40$, $B = 100$.

packets, since the influence of the number of stored packets on the leakage rate diminishes.

In Figs. 19 and 21, the exponential, linear, and constant service rates are compared for $\lambda = 10$. A significant fluctuation is observed in the service outage probability and the mean number of stored energy packets compared to the results in Figs. 17–20. This behavior arises because a higher λ results in more energy packets being stored during daylight hours, leading to increased leakage, particularly at night. Consequently, the stored energy declines sharply during these periods. Since leakage increases with the number of stored energy packets, it is crucial to optimally size the energy harvester to balance energy harvesting and storage, ensuring minimal energy wastage due to excessive leakage.

4. Conclusions and Directions for Future Work

Ideally, many low-power IoT systems could be powered via energy harvesting systems, such as electromagnetic, micromechanical, or piezoelectric generators. However, the effectiveness of such energy harvesting systems can be impaired by the leakage in the corresponding energy storage systems such as batteries or capacitors, including the storage capacity drop of batteries as a function of the number of charge-discharge cycles, the effects of energy leakage, and the charge recovery effects. Thus, to investigate how such effects can be compensated and mitigated, this paper uses modelling techniques to build overall system models of energy storage devices that combine the charge and discharge aspects that are part of battery operation, together with the secondary effects such as capacity drop, energy leakage and charge recovery that impact the sustainability of IoT systems.

Thus, in this paper, we have analysed the impact of such imperfections or non-idealities on the effectiveness of Green IoT nodes and studied the means to compensate for the energy losses caused by energy leakage. Based on a discrete and probabilistic "energy packet" type model, we have computed the outcome of a combination of the rate of power production, energy consumption, and leakage on significant performance metrics such as the service outage probability, the expected energy lifetime of the node and the mean amount of energy stored in the node's battery both at steady-state and in the transitory regime. We have also considered the means to improve these metrics via changes in energy harvester techniques such as photovoltaic or by selecting system operation thresholds, which can interrupt a system's operation when the amount of energy stored moves outside some given thresholds.

The numerical simulations we present provide insight into the negative impact of the energy leakage rate on the energy performance of the IoT node that uses energy storage and renewable energy sources.

We have observed that a linear energy leakage rate degrades the energy performance of such nodes, resulting in an increased probability of service outage, reduced lifetime of the node, and reduced average amount of stored energy, as compared to an exponential leakage characteristic. Indeed, we show in our numerical experiments that the energy leakage rate characteristic, which may be

linear, exponential, or constant, has a very significant impact on the energy performance of the IoT node. We also examine the degree to which the impact of the energy harvesting rate on the lifetime of the node can affect the performance of an IoT node over a 24 hour period with 12 hours of solar radiation (day period) and 12 hours of non-solar radiation (night period) for 50 consecutive days (120 hours).

In future work, we plan to examine how the impact of energy leakage can be mitigated by using various techniques such as Duty Cycling and through techniques that modify the parameters of the communications, including the reduction of packet size, transceiver optimisation, energy-ware routing, adaptive energy-aware sensing, reduction of protocol overhead, voltage and frequency control and Green IoT communication technologies such as BLE, RFID, NFC, Zigbee, LoRa, Sigfox, and other techniques. This work will be accompanied by model refinements based on experimental studies that measure energy leakage rates and feed the measured data into the diffusion models and other mathematical modelling techniques that we use.

References

[1] D. Zhai, M. Sheng, X. Wang, Y. Li, Leakage-aware dynamic resource allocation in hybrid energy powered cellular networks, IEEE Transactions on Communications 63 (2015) 4591–4603.

[2] M. Raeis, A. Burchard, J. Liebeherr, Analysis of a queueing model for energy storage systems with self-discharge, ACM Transactions on Modeling and Performance Evaluation of Computing Systems 5 (2020) 1–26.

[3] G. S. Kuaban, T. Czachórski, E. Gelenbe, S. Sharma, P. Czekalski, A markov model for a self-powered green iot device with state-dependent energy consumption, in: 2023 4th International Conference on Communications, Information, Electronic and Energy Systems (CIEES), 2023, pp. 1–7. doi:10.1109/CIEES58940.2023.10378778.

[4] A. Al-Ansi, A. M. Al-Ansi, A. Muthanna, I. A. Elgendy, A. Koucheryavy, Survey on intelligence edge computing in 6g: Characteristics, challenges, potential use cases, and market drivers, Future Internet 13 (2021).

[5] K. Sadatdiynov, L. Cui, L. Zhang, J. Z. Huang, S. Salloum, M. S. Mahmud, A review of optimization methods for computation offloading in edge computing networks, Digital Communications and Networks 9 (2023) 450–461.

[6] M. H. Alsharif, A. Jahid, A. H. Kelechi, R. Kannadasan, Green iot: A review and future research directions, Symmetry 15 (2023).

[7] A. S. H. Abdul-Qawy, N. M. S. Almurisi, S. Tadisetty, Classification of energy saving techniques for iot-based heterogeneous wireless nodes, Procedia Computer Science 171 (2020) 2590–2599.

[8] M. H. Alsharif, A. Jahid, A. H. Kelechi, R. Kannadasan, Green iot: A review and future research directions, Symmetry 15 (2023) 757.

[9] M. A. Albreem, A. M. Sheikh, M. H. Alsharif, M. Jusoh, M. N. M. Yasin, Green internet of things (giot): applications, practices, awareness, and challenges, IEEE Access 9 (2021) 38833–38858.

[10] G. S. Kuaban, T. Czachórski, E. Gelenbe, P. Pecka, V. Nkemeni, P. Czekalski, Energy performance of internet of things (iot) networks for pipeline monitoring, in: Proceedings of the 20th International Wireless Communications and Mobile Computing Conference (IWCMC 2024), IEEE, 2024 (in press).

[11] E. Gelenbe, Energy packet networks: Ict based energy allocation and storage, in: International Conference on Green Communications and Networking, Springer, 2011, pp. 186–195.

[12] E. Gelenbe, Energy packet networks: adaptive energy management for the cloud, in: CloudCP'12: Proceedings of the 2nd International Workshop on Cloud Computing Platforms, ACM, https://doi.org/10.1145/2168697.2168698, 2012, pp. 1–5.

[13] A. Gautam, S. Dharmaraja, An analytical model driven by fluid queue for battery life time of a user equipment in LTE-A networks, Physical Communication 30 (2018) 213–219.

[14] G. L. Jones, P. G. Harrison, U. Harder, T. Field, Fluid queue models of battery life, in: Proceeding of the 2011 IEEE 19th Annual International Symposium on Modelling, Analysis, and Simulation of Computer and Telecommunication Systems, IEEE, 2011, pp. 278–285. doi:10.1109/MASCOTS.2011.61.

[15] C. Tunc, N. Akar, Markov fluid queue model of an energy harvesting IoT device with adaptive sensing, Performance Evaluation 111 (2017) 1–16.

[16] O. H. Abdelrahman, E. Gelenbe, A diffusion model for energy harvesting sensor nodes, in: 2016 IEEE 24th International Symposium on Modeling, Analysis and Simulation of Computer and Telecommunication Systems (MASCOTS), IEEE, 2016, pp. 154–158.

[17] T. Czachórski, E. Gelenbe, G. S. Kuaban, Modelling energy changes in the energy harvesting battery of an iot device, in: Proceedings of the 2022 30th International Symposium on Modeling, Analysis, and Simulation of Computer and Telecommunication Systems (MASCOTS), IEEE, Nice, France, 2022, pp. 81–88. doi:10.1109/MASCOTS56607.2022.00019.

[18] E. Gelenbe, Y. M. Kadioglu, Battery attacks on sensors: Wireless nodes with battery attacks, in: EuroCybersec 2018: International symposium on computer and information sciences, cybersecurity workshop, Springer Cham, 2018. doi:10.13140/RG.2.2.35482.34241.

[19] G. S. Kuaban, E. Gelenbe, T. Czachórski, P. Czekalski, J. K. Tangka, Modelling of the energy depletion process and battery depletion attacks for battery-powered internet of things (iot) devices, Sensors 23 (2023).

[20] O. P. Angwech, A. S. Alfa, B. Maharaj, Managing the harvested energy in wireless sensor networks: A priority geo/geo/1/k approach with threshold, Energy Reports 8 (2022) 2448–2461.

[21] N. Su, M. Koca, Stochastic transmission policies for energy harvesting nodes with random energy leakage, in: European Wireless 2014; 20th European Wireless Conference, VDE, 2014, pp. 1–6.

[22] N. Dang, R. Valentini, E. Bozorgzadeh, M. Levorato, N. Venkatasubramanian, A unified stochastic model for energy management in solar-powered embedded systems, in: 2015 IEEE/ACM International Conference on Computer-Aided Design (ICCAD), IEEE, 2015, pp. 621–626.

[23] J. Doncel, J.-M. Fourneau, Balancing energy consumption and losses with energy packet network models, in: 2019 IEEE International Conference on Fog Computing (ICFC), IEEE, 2019, pp. 59–68.

[24] E. Gelenbe, Y. M. Kadioglu, Energy loss through standby and leakage in energy harvesting wireless sensors, in: 2015 IEEE 20th International Workshop on Computer Aided Modelling and Design of Communication Links and Networks (CAMAD), IEEEXplore, 2015, pp. 231–236. doi:10.1109/CAMAD.2015.7390515.

[25] Y. M. Kadioglu, E. Gelenbe, Product-form solution for cascade networks with intermittent energy, IEEE Systems Journal 13 (2019) 918–927. doi:10.1109/JSYST.2018.2854838.

[26] S. Samain, J. Doncel, A. Busic, J.-M. Fourneau, Multiclass energy packet networks with finite capacity energy queues, Performance Evaluation 152 (2021) 102228.

[27] S. Samain, J. Doncel, A. Busic, J.-M. Fourneau, Energy packet networks with finite capacity energy queues, in: Proceedings of the 13th EAI International Conference on Performance Evaluation Methodologies and Tools, 2020, pp. 142–149.

[28] A. Bušić, J. Doncel, J. Fourneau, Dynamic load balancing in energy packet networks, Performance Evaluation 165 (2024) 102414.

[29] J. Doncel, J.-M. Fourneau, Energy packet networks with multiple energy packet requirements, Probability in the Engineering and Informational Sciences 35 (2021) 92–110.

[30] I. Kaj, V. Konané, Modeling battery cells under discharge using kinetic and stochastic battery models, Applied Mathematical Modelling 40 (2016) 7901–7915.

[31] T. Zhang, H. Yang, Chapter 7 - high efficiency plants and building integrated renewable energy systems, in: F. Asdrubali, U. Desideri (Eds.), Handbook of Energy Efficiency in Buildings, Butterworth-Heinemann, 2019, pp. 441–595.

[32] A. P. Dobos, PVWatts version 5 manual, Technical Report, National Renewable Energy Lab.(NREL), Golden, CO (United States), 2014.

[33] H. Wang, H. Li, C. Tang, L. Ye, X. Chen, H. Tang, S. Ci, Modeling, metrics, and optimal design for solar energy-powered base station system, EURASIP Journal on Wireless Communications and Networking 2015 (2015) 1–17.

[34] C. Zeljkovic, P. Mrsic, B. Erceg, D. Lekic, N. Kitic, P. Matic, Optimal sizing of photovoltaic-wind-diesel-battery power supply for mobile telephony base stations, Energy 242 (2022) 122545.

[35] M. Ismail, M. Moghavvemi, T. Mahlia, Design of an optimized photovoltaic and microturbine hybrid power system for a remote small community: Case study of palestine, Energy Conversion and Management 75 (2013) 271–281.

[36] J. Ghazanfarian, M. M. Mohammadi, K. Uchino, Piezoelectric energy harvesting: A systematic review of reviews, in: Actuators, volume 10, MDPI, 2021, p. 312.

[37] P. D. Mitcheson, T. C. Green, E. M. Yeatman, A. S. Holmes, Architectures for vibration-driven micropower generators, Journal of microelectromechanical systems 13 (2004) 429–440.

[38] D. W. K. Ng, E. S. Lo, R. Schober, Energy-efficient resource allocation in ofdma systems with hybrid energy harvesting base station, IEEE Transactions on Wireless Communications 12 (2013) 3412–3427.

[39] H. Wang, H. Li, Z. Wang, X. Chen, S. Ci, Stochastic queue modeling and key design metrics analysis for solar energy powered cellular networks, in: 2014 International Conference on Computing, Networking and Communications (ICNC), IEEE, 2014, pp. 472–477.

[40] D. G. Kendall, Stochastic processes occurring in the theory of queues and their analysis by the method of the imbedded markov chain, The Annals of Mathematical Statistics 24 (1953) 338–354.

[41] L. Kleinrock, Queueing Systems Vol. 1: Theory, John Wiley & Sons, 1975.

[42] G. V. Merrett, A. S. Weddell, A. P. Lewis, N. R. Harris, B. M. Al-Hashimi, N. M. White, An empirical energy model for supercapacitor powered wireless sensor nodes, in: 2008 Proceedings of 17th International Conference on Computer Communications and Networks, IEEE, 2008, pp. 1–6.

[43] H. Yang, Y. Zhang, Evaluation of supercapacitor models for wireless sensor network applications, in: 2011 5th International Conference on Signal Processing and Communication Systems (ICSPCS), 2011, pp. 1–6. doi:10.1109/ICSPCS.2011.6140856.

[44] A. S. Weddell, G. V. Merrett, T. J. Kazmierski, B. M. Al-Hashimi, Accurate supercapacitor modeling for energy harvesting wireless sensor nodes, IEEE Transactions on Circuits and Systems II: Express Briefs 58 (2011) 911–915. doi:10.1109/TCSII.2011.2172712.